2024 IEEE/RSJ International Conference on Intelligent Robots and Systems (IROS)
October 14-18, 2024. Abu Dhabi, UAE

Design and implementation of a novel wheel-based cable inspection robot

Hou Mengqi, Jie Li, Fengyu Xu, Lezhi Hu

Abstract— **Regular maintenance and inspection of cables are essential for cable-stayed bridges and suspension bridges, as cables serve as the core components. In order to enable automated detection of cables, this paper proposes a novel wheeled cable inspection robot. The robot utilizes a bilateral wheel structure and is composed of four independent suspension mechanisms. By collaborating with a lifting mechanism, the robot achieves functions such as adhesion, climbing, and obstacle overcoming. The robot is powered by a lithium polymer battery and operated via wireless control by ground personnel. This paper provides a detailed exposition on the structure design and control system of robots, and conducts a mechanical analysis of the suspension mechanism of robots. The maximum obstacle-negotiation height of the robot is calculated, and a mechanical model for cable climbing is established. During prototype testing, the robot demonstrated a mass of 6.7kg, a maximum payload capacity of 6kg, a maximum obstacle height of 10mm, and a fastest climbing speed of 14m/min. These specifications meet the requirements of practical inspections.**

I. INTRODUCTION

Cable-stayed and suspension bridges are widely used in both domestic and international engineering sectors due to their simple design, large spanning capability, and cost-effectiveness. However, the exposed cables of these bridges are susceptible to various environmental factors such as wind, sunlight, rain, and ice. As a result, the cables can experience surface and internal damage, posing a significant risk to the safety of the bridges. Therefore, it is imperative to conduct regular inspections and maintenance on the cables to ensure their integrity [1].

Currently, a range of fully developed cable inspection robots have emerged and started to supplant manual inspection [2]. This not only enhances the efficiency of detection and minimizes the risk, but also mitigates the potential harm to the cable. Out of various climbing techniques, the crawler robot [3], [4] stands out because it can make contact with the cable on a wide surface area and offers excellent climbing stability. However, its slow climbing pace is attributed to its heavy weight. Clamp-type robots [5]–[8] achieve movements by coordinating the grip of their hands with the motion of their body. They can perform multiple actions in a single movement and can adjust their gait to overcome obstacles, exhibiting strong obstacle-negotiation capabilities. But their mobility efficiency is relatively lower. Researchers prefer Wheeled robots [9]–[15] have been extensively designed by numerous researchers due to their ability to move swiftly on cables. However, the attachment mechanism of wheels, which typically involves point or surface contact with the cable, limits the effective payload capacity of these robots due to insufficient stability. Soft robots [16]–[18] achieve movement on cables through the stretching and contracting motion of their flexible bodies. Their lightweight nature results in limited payload capacity, and their unique movement mechanism is not suitable for long-distance movement on cables. The split climbing robot [19], [20] utilize multi-rotors as front-end devices to enable rapid movement and fixation along cables. They employ winches and steel wires to pull the main body towards the front-end device. These robots possess decent mobility speed and payload capacity. However, the overall structure is overly complex, making installation and dismantling cumbersome, and the manufacturing cost is also high.

The robots mentioned above exhibit obvious shortcomings and cannot simultaneously achieve high mobility speed, payload capacity, and obstacle-negotiation capability. In scenarios where carrying large equipment is not required, the convenience of installation and uninstallation, high mobility efficiency, and outstanding obstacle-negotiation ability are important indicators for robots. Therefore, this paper proposes a novel dual-wheeled climbing robot with independent suspension mechanism for efficient inspection of cables. Compared to traditional wheeled robots, this design prioritizes the rapid installation and uninstallation of robots onto cables, and also emphasizes the ability to move swiftly even when carrying heavy loads. The modular independent suspension mechanism is easy to replace, and the flexible suspension structure also allows the robot to have a good ability to overcome obstacles. The lightweight design not only facilitates portability but also reduces costs, making it suitable for deployment in engineering applications.

II. ROBOT DESIGN

In this section, a comprehensive elaboration is provided on the robot's overall structural design and its core suspension mechanism. Furthermore, the process of single-person independent installation of the robot is also discussed in detail.

This work was supported in part by the National Natural Science Foundation of China under Grant 52175100, the Natural Science Foundation of Jiangsu Province, China (Grant No. BK202300367), the Natural Science Foundation of the Jiangsu Higher Education (Grant No. 23KJB510016), and Science and Technology Project of the State Administration for Market Regulation, China (Grant No. 2023MK040).

Mengqi Hou, Jie li, Fengyu Xu and Lezhi Hu are with the College of Automation and College of Artificial Intelligence, Nanjing University of Posts and Telecommunications, Nanjing 210023, China(e-mail: houmengqi22@163.com, jieli@njupt.edu.cn, xufengyu598@163.com, 326075282@qq.com,). Corresponding author: Fengyu Xu.

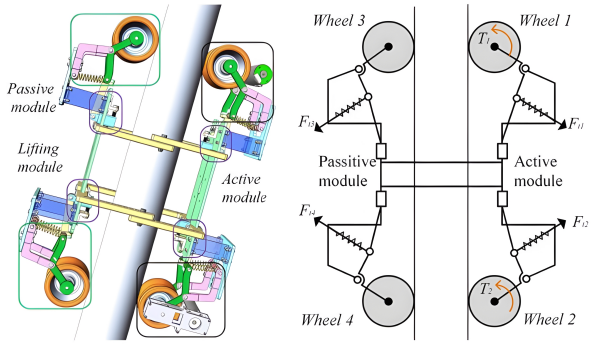

Fig. 1. The 3D model and mechanical schematic of the robot

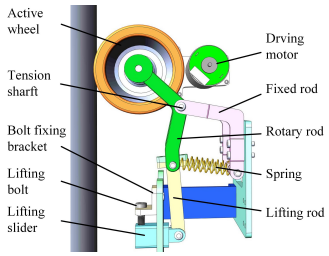

Fig. 2. The 3D model of the suspension mechanism and lifting mechanism

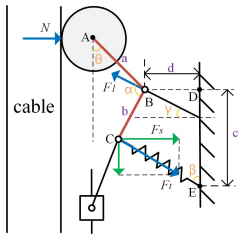

Fig. 3. Analysis for installation

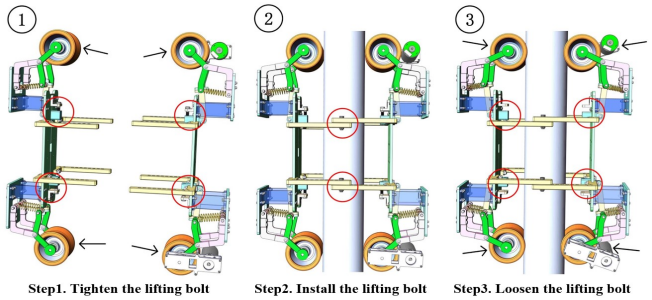

Fig. 4. The installation steps for the robot

A. Mechanical structure design

The novel designed independent suspension cable climbing robot (Fig. 1) in this paper consists primarily of four climbing modules and four lifting modules. The central structure of the robot is concave inward to accommodate the installation of control systems and detection devices. The structures symmetrically arranged on both sides along the cable are connected by ”L”-shaped rods. By altering the connection holes of the ”L”-shaped rods, the robot can climb cables of different diameters. The climbing modules comprise active climbing modules and passive climbing modules, the difference being that active climbing modules have drive motors and transmission structures, with two identical modules installed as a pair at both ends of the framework. One end of the lifting module can slide up and down within a certain distance in the body groove, while the other end is connected to the multi-link suspension mechanism of the climbing module. By applying tension force F_t to the wheels through springs on the suspension mechanism, the wheels are pressed against the cable surface, resulting in frictional forces along the cable that allow adhesion. The combination of the multi-link suspension mechanism and the lifting mechanism enables the suspension structure to generate a significant range of flexible deformation, facilitating functions such as installation, uninstallation, and obstacle-negotiation. To ensure the stability of the mechanism, we have implemented a design where two tension springs are symmetrically arranged along both sides of the central plane of the lifting rod.

The suspension mechanism of the robot (Fig. 2) consists of a fixed rod connected to the body, tension springs, a tension shaft, and a rotary rod. In this case, the rotary rod is connected to the shaft of the ”V”-shaped wheel and the tension shaft at each extremity, and the center is connected to the fixed rod. The lifting mechanism consists of a lifting bolt, a bolt-fixing bracket, a lifting slider, and a lifting rod. One extremity of the lifting rod is connected to the lifting slide, and the other extremity is connected to the tension shaft. When the lifting bolt is tightened, the lifting slider moves along the sliding groove towards the bolt-fixing bracket, causing the lifting rod to move upward, stretching the spring in the process. The restoring force of the spring is then utilized to provide the spring preload force.

B. Process of installation

A single individual may install and remove the robot without any supplementary clamps. The installation procedure comprises three sequential steps in Fig. 4. (1) By tightening the lifting bolts of the four lifting mechanisms, as the lifting rods rise, the springs are stretched, causing the four wheels to spread outward. (2) By fastening the mechanisms on both sides to the cable using bolts, ensure that the ”V”-shaped grooves on the wheels are aligned with the cable. At this moment, there exists a minute gap between the wheel and the cable, allowing the wheel to slide slightly on the cable. (3) By loosening the four lifting bolts, under the tension of the springs, the four wheels move inward, exerting sufficient pressure on the cable to make the robot adhere to the surface of the cable.

III. Kinematics Analysis

The robot needs to hold, move and overcome obstacles on cables and to illustrate the feasibility of these functions, this section analyses the robot’s mounting mechanics, obstacle-negotiation capabilities and climbing conditions.

A. Mechanical analysis of installation

As inferred from the previous context, after mounting the robot onto a cable, the removal of lifting bolts results in the wheels exhibiting an inward movement tendency under the influence of the suspension and lifting mechanisms. Consequently, the wheels experience pressure from the cable, generating the necessary frictional force for adhesion. Taking the active wheel as an example, a kinematic analysis of the mounting process can be performed, neglecting the wheel

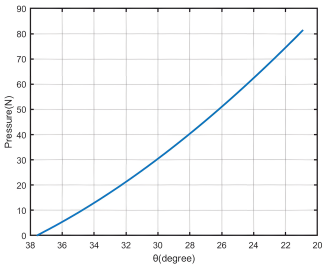

Fig. 5. The relationship between N and θ

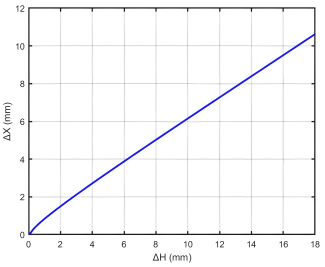

Fig. 6. The relationship between ΔX and ΔH

TABLE I

THE DIMENSION OF SUSPENSION MECHANISM

a	$46mm$	d	$48mm$
b	$50mm$	α	$120°$
c	$58mm$	γ	$10°$

displacement during this process. As shown in Fig. 3, the relationship between the installation angle of the wheel θ and the length of the spring l_1 can be obtained:

$$\begin{cases} sin\beta = (d + b\ sin(\alpha + \theta))/l_1 \\ -cos(\alpha + \theta) = (c - l_1\ cos\beta)/b \end{cases} \tag{1}$$

Where point D is the projection of point B on the frame position of the robot, and point E is the spring fixation point. a and b are the lengths of rod AB and rod BC respectively, c and d are the lengths of DE and BD respectively, θ is the angle between rod AB and the axis of the cable, α is the angle between rod AB and rod BC, and β is the angle between the spring and the fuselage in the vertical direction. The force balance equation of the curved link ABC can be written as follows:

$$\begin{cases} \sum F_x = F_1\ cos\gamma - N - F_t\ sin\beta = 0 \\ \sum F_y = F_1\ sin\gamma - F_t\ cos\beta = 0 \end{cases} \tag{2}$$

In the formula, the spring tension force F_t can be written as:

$$F_t = kx = k(l_1 - l_1') \tag{3}$$

where l_1' is the original length of the spring, k is the spring constant, and x is the elongation of the spring. Combining formula (2), the pressure N is as follows:

$$N = F_t \left(\frac{cos\beta}{tan\gamma} - sin\beta \right) \tag{4}$$

The dimensional parameters of the robot are shown in Table 1, and as θ changes, the pressure N and the spring tension F_t change, as shown in Fig. 5. Assuming the coefficient of adhesion between the rolling wheel and the cable is $\mu = 0.4$, then, the robot can be fixed on the cable when θ reaches 27°.

B. Obstacle-negotiation performance analysis

The suspension and lifting mechanisms can provide spring preload force and make the climbing mechanism produce flexible deformation to overcome the obstacle.

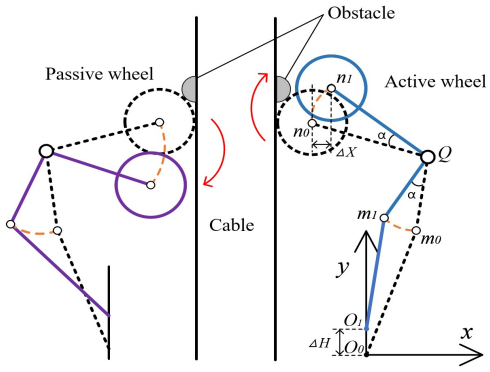

Fig. 7. Analysis for obstacle overcoming

The obstacle-negotiation process of the active and passive wheels is illustrated in Fig. 7. Taking the active wheel as an example, after the robot is installed on the cable, a coordinate system is established with the position O_0 at the bottom of the lifting rod as the origin. The vertical direction is defined as the X-axis, while the direction along the cable is defined as the Y-axis. When the lifting pole ascends by a height ΔH, moving from O_0 to O_1, the rotary rod attached to the wheel rotates at point $Q(x_q,y_q)$ by an angle α, then the bottom of rotary rod rotates from m_0 to m_1, the wheel center moves from n_0 to n_1, and the wheel undergoes a horizontal displacement of length ΔX.

The coordinates of point m_0 are known, and the coordinates of point m_1 are given as follows:

$$\begin{cases} x^2 + (y - \Delta H)^2 = {l_0}^2 \\ (x - x_q)^2 + (y - y_q)^2 = {l_1}^2 \end{cases} \tag{5}$$

Where l_0 and l_1 are the lengths of the lifting rod and the lower half of the rotary rod, respectively. The rotation angle α of the rotary rod is obtained as follows:

$$\alpha = arccos \left(\frac{\overrightarrow{\mathrm{Qm_1}} \cdot \overrightarrow{\mathrm{Qm_0}}}{|\mathrm{Qm_1}| \cdot |\mathrm{Qm_0}|} \right) \tag{6}$$

The coordinates of point n_o are known, and the coordinates of point n_1 are given as follows:

$$\begin{cases} n_{1x} = Q_x + cos\alpha(n_{0x} - Q_x) - sin\alpha(n_{0y} - Q_y) \\ n_{1y} = Q_y + sin\alpha(n_{0x} - Q_x) + cos\alpha(n_{0y} - Q_y) \end{cases} \tag{7}$$

From (5), (6), and (7), the coordinates of the known points are obtained in the 3D model, which allows us to establish the relationship between the upward displacement ΔH of the active lifting rod and the length of the wheel opening ΔX, as shown in Fig. 6.

When the passive wheel comes into contact with an obstacle, the resistance from the obstacle acting on it in the climbing direction is greater than the support force from the suspension mechanism. As a result, the passive wheel contracts inwardly, the extension of the spring changes, and at the same time, the lifting slider moves downward until

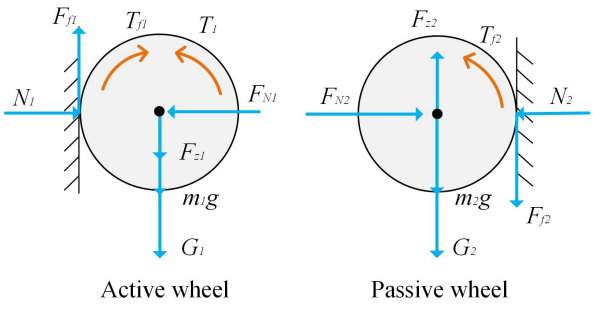

Fig. 8. Force–torque analysis on the active wheel and passive wheel.

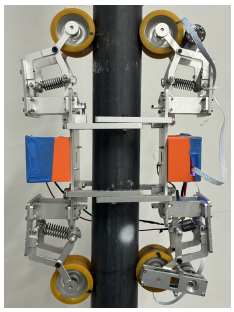

Fig. 9. The prototype of robot

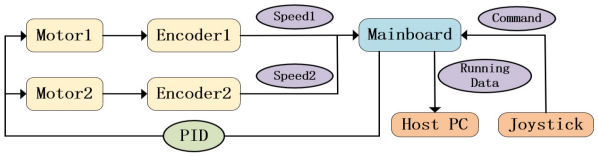

Fig. 10. Control system

the passive wheel forms a sufficient clearance on the surface of the tension cable. After the installation of the prototype, it was measured that the lifting rod of the active wheel can achieve an elevation height of approximately 18mm. This implies a theoretical maximum obstacle traversal height of around 11mm for the active wheel, and similarly, an estimated maximum obstacle traversal height of approximately 10mm for the passive wheel. These values will be validated in subsequent prototype testing.

C. Mechanical analysis of climbing force

One side of this design is the active wheel and the other side is the passive wheel. Taking the upward movement as an example, the forces on the active and passive wheels are analyzed separately and the critical driving conditions are obtained.

The climbing force analysis of the active and driven wheels is shown in Fig. 8, and the equilibrium model of the force and moment of the active wheel is:

$$\begin{cases} F_{f1} - F_{z1} - m_1 g - G_1 = 0 \\ T_1 - F_{f1} \cdot r - T_{f1} = 0 \end{cases} \tag{8}$$

Where F_{N1} and N_1 represent the pressure in the horizontal direction. F_{z1} and F_{f1} are the static friction force on the active wheel and the resistance of the cable to the active wheel respectively, G_1 is the gravity force on the active wheel, T_1 and T_f are the driving and resistance torque respectively, m_1 is the mass of the active wheel, and r is the radius of the wheel. The equilibrium model of the force and moment of the passive wheel is:

$$\begin{cases} F_{z2} - m_2 g - G_2 - F_{f2} = 0 \\ F_{f2} \cdot r - T_{f2} = 0 \end{cases} \tag{9}$$

Where F_{z2} is the support force on the passive wheel, m_2 is the mass of the passive wheel, G_2 is the gravity force on the passive dynamic wheel, F_{f2} is the friction force of the cable on the passive wheel, and T_{f2} is the friction torque. When climbing upwards, enough driving torque is needed to ensure the normal climbing of the device, and the rising condition is:

$$T_1 \geq T_{f1} + T_{f2} + (m_1 g + G_1 + m_2 g + G_2) r \tag{10}$$

Combining formula (4) with the active wheel as an example, the relationship between the spring preload force for and the mounting angle is obtained for the robot's holding condition:

$$m_1 g + G_1 = Ft \cdot \mu (cos\beta_1 / tan_1 - sin\beta_1) \tag{11}$$

IV. Experiments

This section presents the prototyping of the robot, along with a detailed experimental process and its corresponding results, aimed at validating the design of the robotic system.

The prototype of the robot is shown in Fig. 9. The main structural components of the robot were made of 6061 aluminum alloy and subjected to surface anodic oxidation treatment, providing excellent strength and corrosion resistance. Weight reduction holes optimization were applied to the main body parts. The driving mechanism employed a DC geared motor with a Hall encoder, with a motor reduction ratio of 1:27 and a rated torque of 13.5 kg.cm. A synchronized gear with a transmission ratio of 3:2 was used to drive the "V"-shaped wheels, which were coated with butyl rubber to increase the coefficient of adhesion with the cable surface. Furthermore, to counteract potential deflection in the robot's trajectory caused by cable rotation, an anti-bias structure has been devised.

The control system of the climbing robot consists of a motion control system and a ground host, as shown in Fig. 10. The motion control system consists of a control board based on STM32, a signal receiving module, and DC motors. Hall encoders are used to read the current rotational speed of the motor. The control board performs calculations based on the received command signal, and utilizes incremental PID control to adjust the motor speed. The ground host can also read parameters such as motor speed, direction, and current to monitor the real-time state of the motor.

In the laboratory, instead of a cable, a plastic pipe with a diameter of 90mm was used to complete a climbing speed

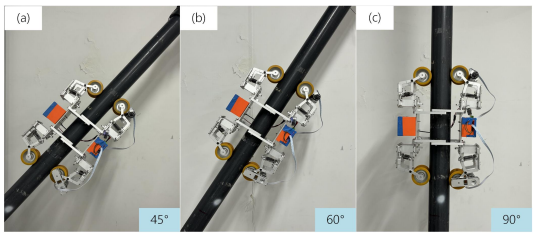

Fig. 11. Climbing and falling experiment

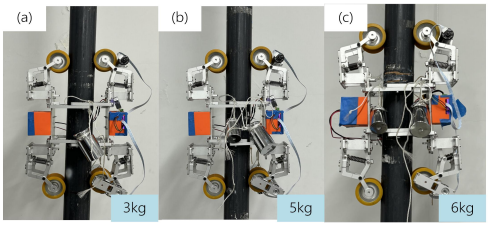

Fig. 13. Payload experiment

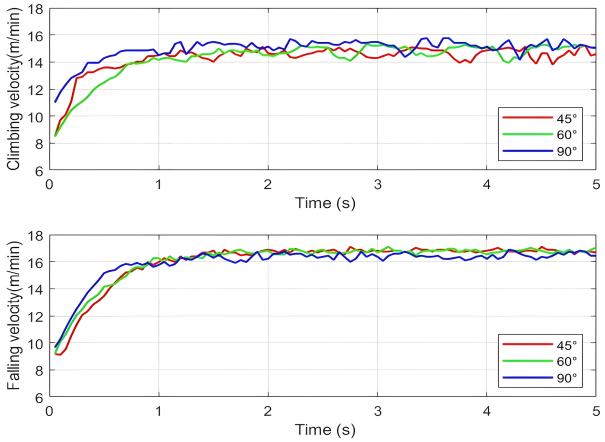

Fig. 12. Velocity in climbing and falling experiment

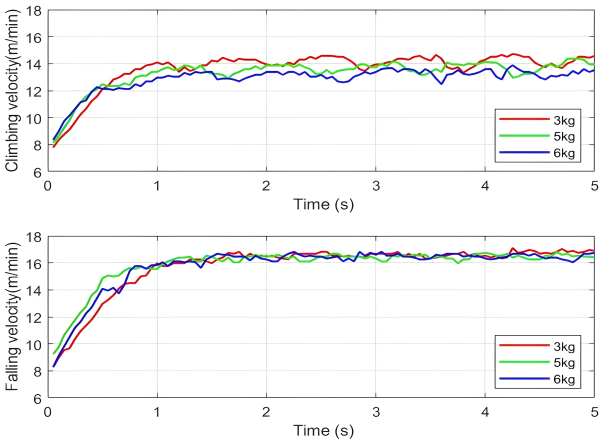

Fig. 14. Velocity in payload experiment

experiment, a payload capacity experiment, and an obstacle-negotiation experiment.

A. *Climbing and Falling experiment*

Experiments were conducted with different cable inclinations of 45°, 60°, and 90°, as depicted in Fig. 11. The velocity of ascent and descent was recorded using encoders.

From Fig. 12, it can be seen that in the case of no load, the climbing velocity of the robot is maintained at about 14m/min, and the falling velocity is maintained at about 16m/min. With the increase of inclination angle, the motion speed of the robot does not change significantly, which indicates that the robot can be stably adsorbed on the cable.

B. *Payload experiment*

By adding weights on both sides of the robot, a payload capacity experiment was carried out with the tension cable tilted at 90°, as shown in Fig. 13, recording the climbing and falling velocity of the robot under different loads and observing whether there is any slippage.

The results in Fig. 14 show that the load mass is within 3kg, and there is no significant change in the robot's rising speed; when the load mass is between 3kg and 6kg, the robot's rising speed starts to slow down, but it can still be operated stably. As the load continues to increase, the robot will experience slipping during climbing, and due to the use of weights as the payload, the load distribution on the robot becomes uneven, resulting in a certain degree of angular deflection. For a robot with a self-mass of only 6.7 kg, the payload reaches 6 kg, yielding an effective payload ratio of about 90%.

C. *Obstacle-negotiation experiment*

The cable is braided with multi-stranded steel ropes, and its surface is uneven, with obstacles such as cable clamps present. Therefore, the climbing device is required to possess a certain level of obstacle-negotiation capability. As shown in Fig. 15, with the cable inclination angle of 90°, ring-shaped obstacles with diameters of 5mm, 8mm and 10mm are fixed on the cable. The circular obstacles we designed can represent barriers of different heights, and the rectangular obstacles exhibit similarities to shorter circular obstacles. To make the test conditions even more stringent, a large battery close to 1kg was mounted on the robot, and the obstacle-crossing experiments were performed at a speed of 14m/min. The results in Fig. 16 illustrate the change in speed of both the active and driven wheels as they pass through the obstacle.

By utilizing the numerical detection from the encoder on the active wheel, the situation of obstacle traversal by the robot can be assessed. As the passive wheel relies on resistance torque for obstacle traversal, the exerted force on the cable during the traversal induces certain vibrations in the cable, as evident in the accompanying video footage. However, due to the action of the spring force, the robot is capable of swift recovery, and the climbing process remains unaffected by cable vibrations. The obtained results demonstrate that both the active and passive wheels of the robot

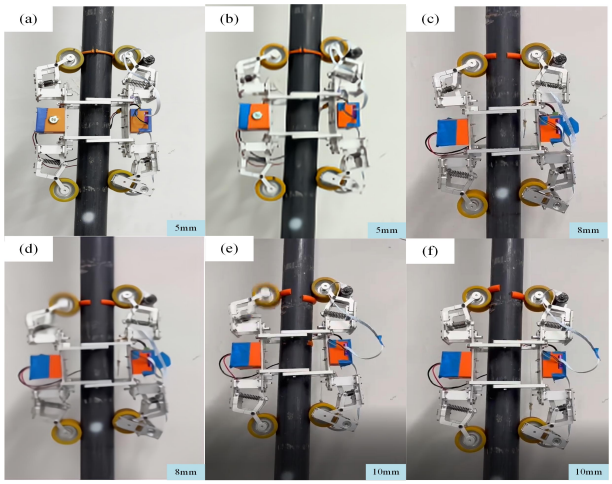

Fig. 15. Obstacle-negotiation experiment

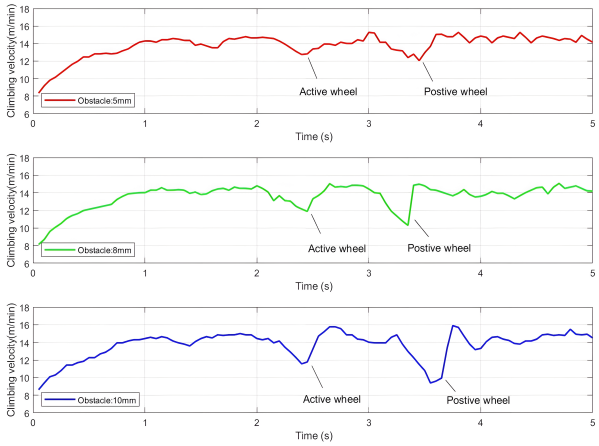

Fig. 16. Velocity in obstacle-negotiation experiment

are capable of overcoming obstacles with a height of 10mm, aligning with the theoretical analysis.

V. CONCLUSIONS

This study presents the design of a lightweight and portable cable climbing robot. By integrating the flexible suspension module with the lifting module, the installation and disassembly of the robot are made more convenient. The mechanical model for the robot's installation and obstacle traversal is analyzed, and the critical climbing conditions are calculated. In the prototype experiment, the robot weighs only 6.7kg and can carry a payload of 6kg. It demonstrates the capability to overcome obstacles of up to 10mm in height, showcasing excellent performance. The subsequent work of this paper aims to address the issue of robot deflection caused by uneven distribution of heavy loads encountered during experiments, and to conduct tests on actual cables under outdoor wind loading conditions.

REFERENCES

[1] H.-B. Yun, S.-H. Kim, L. Wu, J.-J. Lee *et al.*, "Development of inspection robots for bridge cables," *The Scientific World Journal*, vol. 2013, 2013.

[2] Y. Tian, C. Chen, K. Sagoe-Crentsil, J. Zhang, and W. Duan, "Intelligent robotic systems for structural health monitoring: Applications and future trends," *Automation in construction*, vol. 139, p. 104273, 2022.

[3] K. H. Cho, Y. H. Jin, H. M. Kim, and H. R. Choi, "Development of novel multifunctional robotic crawler for inspection of hanger cables in suspension bridges," in *2014 IEEE international conference on robotics and automation (ICRA)*. IEEE, 2014, pp. 2673–2678.

[4] K. H. Cho, Y. H. Jin, H. M. Kim, H. Moon, J. C. Koo, and H. R. Choi, "Multifunctional robotic crawler for inspection of suspension bridge hanger cables: Mechanism design and performance validation," *IEEE/ASME Transactions on Mechatronics*, vol. 22, no. 1, pp. 236–246, 2016.

[5] M. Tavakoli, A. Marjovi, L. Marques, and A. T. de Almeida, "3dclimber: A climbing robot for inspection of 3d human made structures," in *2008 IEEE/RSJ International Conference on Intelligent Robots and Systems*. IEEE, 2008, pp. 4130–4135.

[6] Z. Zheng, S. Hu, and N. Ding, "A biologically inspired cable climbing robot: Ccrobot-design and implementation," in *2018 IEEE International Conference on Robotics and Biomimetics (ROBIO)*. IEEE, 2018, pp. 2354–2359.

[7] Z. Zheng and N. Ding, "Design and implementation of ccrobot-ii: a palm-based cable climbing robot for cable-stayed bridge inspection," in *2019 International Conference on Robotics and Automation (ICRA)*. IEEE, 2019, pp. 9747–9753.

[8] Q. Fu, Y. Guan, and H. Zhu, "A novel robot with rolling and climbing modes for power transmission line inspection," in *2022 IEEE/RSJ International Conference on Intelligent Robots and Systems (IROS)*. IEEE, 2022, pp. 7122–7128.

[9] Q. Zhao, Z. Jiang, and H. K. Chu, "A soft-rigid air-propelled pipe-climbing robot," in *2021 IEEE International Conference on Robotics and Automation (ICRA)*. IEEE, 2021, pp. 11 850–11 855.

[10] W. X. XU FY and P. CAO, "Design and application of a new wheel-based cable inspection robot [c]," in *2011 IEEE International Conference on Robotics and Automation (ICRA). Shanghai: IEEE*, 2011, pp. 4909–4914.

[11] F. Xu, S. Dai, Q. Jiang, and X. Wang, "Developing a climbing robot for repairing cables of cable-stayed bridges," *Automation in Construction*, vol. 129, p. 103807, 2021.

[12] K. H. Cho, H. M. Kim, Y. H. Jin, F. Liu, H. Moon, J. C. Koo, and H. R. Choi, "Inspection robot for hanger cable of suspension bridge: Mechanism design and analysis," *IEEE/ASME Transactions on mechatronics*, vol. 18, no. 6, pp. 1665–1674, 2013.

[13] Y. Wang, X. Li, M. Yang, and F. Yin, "Design and implementation of the wheel-clamping stay cable inspection robot," *Advances in Mechanical Engineering*, vol. 15, no. 8, p. 16878132231194409, 2023.

[14] P. Gui, L. Tang, and S. Mukhopadhyay, "A novel robotic tree climbing mechanism with anti-falling functionality for tree pruning," *Journal of Mechanisms and Robotics*, vol. 10, no. 1, p. 014502, 2018.

[15] F. Lv, F. Xu, and C. Wu, "The obstacle-surmounting performance of a cable-climbing robot," in *2019 IEEE/ASME International Conference on Advanced Intelligent Mechatronics (AIM)*. IEEE, 2019, pp. 960–965.

[16] B. Liao, H. Zang, M. Chen, Y. Wang, X. Lang, N. Zhu, Z. Yang, and Y. Yi, "Soft rod-climbing robot inspired by winding locomotion of snake," *Soft robotics*, vol. 7, no. 4, pp. 500–511, 2020.

[17] R. Li, Y. Liu, A. Guo, M. Shou, M. Zhao, D. Zhu, P.-a. Yang, and C.-H. Lee, "An inchworm-like climbing robot based on cable-driven grippers," *IEEE/ASME Transactions on Mechatronics*, 2023.

[18] G. Singh, S. Patiballa, X. Zhang, and G. Krishnan, "A pipe-climbing soft robot," in *2019 International Conference on Robotics and Automation (ICRA)*. IEEE, 2019, pp. 8450–8456.

[19] N. Ding, Z. Zheng, J. Song, Z. Sun, T. L. Lam, and H. Qian, "Ccrobot-iii: a split-type wire-driven cable climbing robot for cable-stayed bridge inspection," in *2020 IEEE International Conference on Robotics and Automation (ICRA)*. IEEE, 2020, pp. 9308–9314.

[20] Z. Zheng, W. Zhang, X. Fu, S. Hazken, X. Hu, H. Chen, J. Luo, and N. Ding, "Ccrobot-iv: An obstacle-free split-type quad-ducted propeller-driven bridge stay cable-climbing robot," *IEEE Robotics and Automation Letters*, vol. 7, no. 4, pp. 11 751–11 758, 2021.